Available online at www.sciencedirect.com
SCIENCE DIRECT
Polymer 47 (2006) 527–538
polymer
www.elsevier.com/locate/polymer

Synthesis and characterization of new fluorene-acceptor alternating and random copolymers for light-emitting applications

Wen-Chung Wu [a], Cheng-Liang Liu [a], Wen-Chang Chen [a,b,*]

[a] Department of Chemical Engineering, National Taiwan University, No. 1, Sec. 4, Roosevelt Road, Taipei 106, Taiwan, ROC
[b] Institute of Polymer Science and Engineering, National Taiwan University, Taipei 106, Taiwan, ROC

Received 21 September 2005; received in revised form 17 November 2005; accepted 18 November 2005
Available online 7 December 2005

Abstract

A series of novel light-emitting copolymers consisted of 9,9-dihexylfluorene (**F**) and different acceptor segments, including quinoxaline (**Q**), 2,1,3-benzothiadiazole (**BT**) and thieno[3,4-*b*]-pyrazine (**TP**), were synthesized by the palladium-catalyzed Suzuki coupling reaction. Three fluorene-acceptor alternating copolymers (**PFQ**, **PFBT**, **PFTP**) and six **F**-**TP** (**PFTP0.5**–**PFTP35**) random copolymers were investigated and compared with the parent polyfluorene (**PF**). The experimental results suggest that the acceptor strength or content significantly affect the electronic and optoelectronic properties. The optical absorption maxima of the **PF**, **PFQ**, **PFBT**, and **PFTP** are 368, 416, 470, and 578 nm, respectively, which indicates the significance of intramolecular charge transfer. The electrochemical band gap also shows a similar trend. The incorporation of the acceptor into the **PF** lowers the LUMO level and thus could improve the electron-accepting ability of the **PF**. The emission maxima on the photoluminescence (PL) spectra of the **PF**, **PFQ**, **PFBT**, and **PFTP** films are 424, 493, 540, and 674 nm, which correspond to the color of blue, green, yellow, and red, respectively. It suggests that the full color of emission can be achieved by different acceptors. The significant positive solvatochromism on the PL spectra in different polar solvents suggests the efficient intramolecular charge transfer in **PFTP**. However, such charge transfer or heavy-atom effect results in fluorescence quenching and thus reduces the PL efficiencies. By random copolymerizing the **TP** into the **PF**, the PL efficiency could be improved. A significantly reduction on the **PF** emission peak with increasing the **TP** content suggests the energy transfer between the **PF** and **TP** segments. Besides, the characteristics on the electroluminescence (EL) devices of ITO/PEDOT:PSS/emissive layer/Ca/Ag suggest that such energy transfer results in the complete quenching of the **PF** emission at only 1% **TP** content in the **PFTP01**. The maximum external quantum efficiency (EQE) of the EL device based on the **PFTP01** is superior to that of the **PF** due to the reduced LUMO level in matching with the Ca. The CIE 1931 coordinates of the **PFTP01** based EL device under the condition of maximum EQE is (0.66, 0.31), which is close to the standard red of (0.66, 0.34) demanded by the National Television System Committee (NTSC). The luminescence characteristics based on the prepared polymers depend on the Förster energy transfer or the intramolecular charge transfer, or heavy-atom fluorescence quenching. The present study suggests that the tuning of the electronic and optoelectronic properties could be achieved by incorporating various acceptors or content into the polyfluorenes.

Keywords: Polyfluorene; Charge transfer; Luminescence

1. Introduction

Conjugated polymers have been extensively studied for their potential applications in electroluminescence displays [1,2], photovoltaic devices [3,4], and thin film transistors [5–7]. They not only combine the physical properties of polymers with those of semiconductors to obtain unique and novel materials but also provide tunable electronic and/or mechanical properties by structure modification [8]. The band structures of conjugated polymers can be manipulated by minimization of bond length alternation [9,10] and incorporation of donor–acceptor units [11,12], which are key to tune their electronic and optoelectronic properties. We are particularly interested in the donor–acceptor alternating copolymers since their electronic properties are tuned efficiently by intramolecular charge transfer (ICT) [11–14].

Polyfluorenes (**PFs**) have been widely studied for polymer light-emitting diodes (PLED) because of their processibility, high quantum yield, and good charge transport properties [15]. However, the poor electron-transporting property of polyfluorene results in a large electron-injection barrier and unbalance

* Corresponding author. Address: Department of Chemical Engineering, National Taiwan University, No. 1, Sec. 4, Roosevelt Road, Taipei 106, Taiwan, ROC. Tel.: +886 2 23628398; fax: +886 2 23623040.
E-mail address: chenwc@ntu.edu.tw (W.-C. Chen).

0032-3861/$ - see front matter © 2005 Elsevier Ltd. All rights reserved.
doi:10.1016/j.polymer.2005.11.058

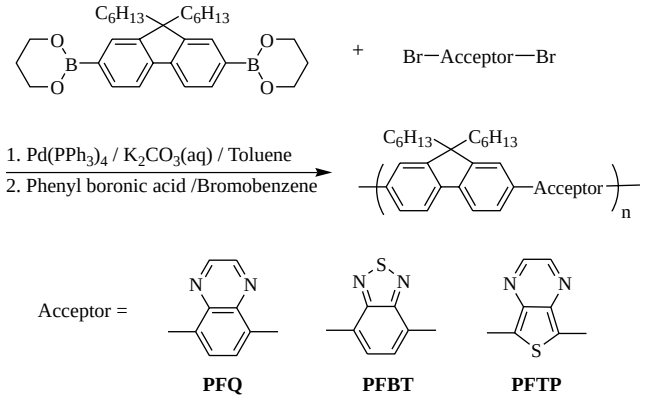

Scheme 1. Synthesis of the fluorene-acceptor alternating copolymers, **PFQ**, **PFBT**, and **PFTP**.

of charge carrier transport for the PLED application. Therefore, copolymerization of fluorene with various electron-accepting and/or electron-transporting moieties has been investigated to improve this shortcoming [16]. Recently, donor–acceptor conjugated copolymers based on fluorene with various acceptors were reported in the literature, including benzothiadiazole [16], pyridine [17], bithiazole [18], naphthoselenadiazole [19], indenofluorene [20], quinoxaline [21], and perylene [22]. The light-emitting color or efficiency of PLED based on the fluorene-acceptor copolymers were easily tuned by the acceptors. Besides, photovoltaic devices with good efficiencies were demonstrated by poly(9,9-dioctylfluorene-*alt*-benzothiadiazole) (F8BT) [23]. High electron mobility from the F8BT-based field effect transistor was also reported recently [24].

Although various fluorene based donor–acceptor copolymers have shown tunable optoelectronic properties and promising device applications, the effects of the acceptor strength on the optoelectronic properties have not been addressed yet. In this study, three fluorene-acceptor alternating and six random conjugated copolymers were synthesized using palladium(0)-catalyzed Suzuki coupling reaction and compared, as shown in Schemes 1 and 2, respectively. The physical properties of the synthesized donor–acceptor conjugated polymers were compared with those of the parent poly[2,7-(9,9-dihexylfluorene)] (**PF**). The studied acceptors included quinoxaline (**Q**), 2,1,3-benzothiadiazole (**BT**) and thieno[3,4-**b**]pyrazine (**TP**). The LUMO of the **Q**, **BT**, and **TP** are −0.90, −1.81, and −1.41 eV, respectively [25], which indicates the order of the acceptor strength is **BT** > **TP** > **Q**. Thus, the effects of acceptor strength and intramolecular charge transfer between fluorene and acceptor segments on the optoelectronic properties can be explored. Besides, six fluorene-**TP** random copolymers were synthesized for investigating the effects of the **TP** content on the optoelectronic properties. The feeding ratios of the 9,9-dihexylfluorene-2,7-bis(trimethyleneborate) and 9,9-dihexyl-2,7-dibromofluorene to the **TP** are 99.5:0.5, 99:1, 95:5, 85:15, 75:25, and 65:35 for the random copolymers of **PFTP0.5**, **PFTP01**, **PFTP05**, **PFTP15**, **PFTP25**, and **PFTP35**, respectively. Electroluminescence (EL) devices fabricated from the synthesized polymers as emissive layers were characterized. The possible energy transfer from the fluorene to fluorene-acceptor segment was investigated. The color tuning ability of the EL devices through various acceptors or content was also demonstrated in this study.

2. Experimental

2.1. Materials

2,1,3-Benzothiadiazole, bromine, glacial acetic acid, zinc dust, glyoxal (40 wt% in water), 3,4-diaminothiophene dihydrochloride, *N*-bromosuccinimide, 9,9-dihexylfluorene-2,7-bis(trimethyleneborate), 9,9-dihexyl-2,7-dibromofluorene, tetrakis(triphenylphosphine)-palladium(0), potassium carbonate, and trioctylmethylammonium chloride (aliquat® 336), were purchased from Aldrich (Missouri, USA) or Acros (Geel, Belgium) and used without further purification. Ultra-anhydrous solvents used in the reactions were purchased from Tedia (Ohio, USA). The following acceptor monomers were prepared according to literature procedures: 4,7-dibromo-2,1,3-benzothiadiazole [26], 5,8-dibromoquinoxaline [27,28], and 5,7-dibromothieno[3,4-*b*]-pyrazine [29,30].

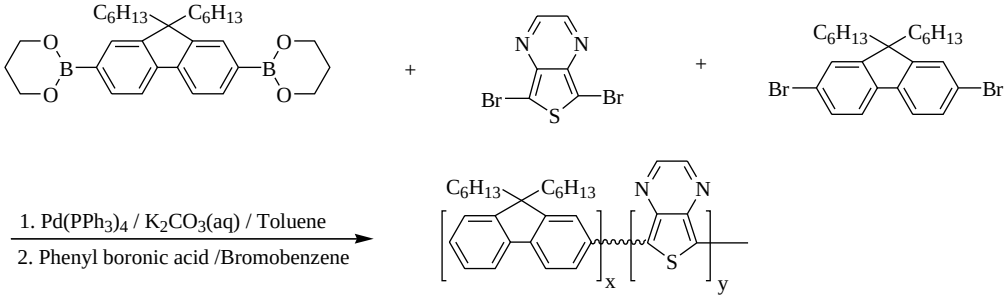

x : y = 99.5 : 0.5, **PFTP0.5**
99 : 1, **PFTP01**
95 : 5, **PFTP05**
85 : 15, **PFTP15**
75 : 25, **PFTP25**
65 : 35, **PFTP35**

Scheme 2. Synthesis of the fluorene–**TP** copolymers, **PFTP0.5**–**PFTP35**.

2.2. General procedure of polymerization

The general procedure of synthesizing fluorene-acceptor alternating copolymers is shown in Scheme 1. 9,9-Dihexylfluorene-2,7-bis(trimethyleneborate), acceptor monomer (**Q**, **BT**, or **TP**), tetrakis(triphenylphosphine)palladium(0) (1 mol% with respect to diborate monomer), and several drops of aliquat® 336 were dissolved in toluene. To the reaction mixture, degassed aqueous 2 M K_2CO_3 (3.3 equiv. with respect to the diborate monomer) was added. The mixture was refluxed with vigorous stirring for 72 h under a nitrogen atmosphere. The end groups were capped by refluxing for 12 h each with phenyl boronic acid and bromobenzene (both 1.1 equiv. with respect to diborate monomer). After endcapping, the mixture was cooled and poured into a mixture of methanol and water. The precipitated material was dissolved into a small amount of THF and then re-precipitated into methanol to afford crude polymer. The crude polymer was washed for 24 h with acetone to remove oligomers and catalyst residues.

The general procedure of synthesizing fluorene-**TP** random copolymers is shown in Scheme 2. The same steps were used except for adding different ratios of 9,9-dihexyl-2,7-dibromofluorene and 5,7-dibromothieno[3,4-*b*]pyrazine instead of 5,7-dibromothieno[3,4-*b*]pyrazine only. The specific polymerization formulation, conditions, and structural characterization are described as below.

2.2.1. Poly[2,7-(9,9-dihexylfluorene)] (*PF*)

502 mg of 9,9-dihexylfluorene-2,7-bis(trimethyleneborate) (1 mmol), 492 mg of 9,9-dihexyl-2,7-dibromofluorene (1 mmol), and 10 ml of toluene were used to afford 600 mg of light yellow solid (90.3%). ^{1}H NMR ($CDCl_3$), δ (ppm): 0.80 (br, 10H), 1.15 (br, 12H), 2.15 (br, 4H), 7.68–7.86 (m, br, 6H). ^{13}C NMR ($CDCl_3$), δ (ppm): 14.02, 22.56, 23.85, 29.67, 31.46, 40.36, 55.33, 119.98, 121.52, 126.15, 140.02, 140.53, 151.81. Anal. Calcd for $C_{25}H_{32}$ (%): C, 90.30; H, 9.70. Found: C, 89.76; H, 9.60.

2.2.2. Poly[2,7-(9,9′-dihexylfluorene)-alt-5,8-quinoxaline] (*PFQ*)

251 mg of 9,9-dihexylfluorene-2,7-bis(trimethyleneborate) (0.5 mmol), 144 mg of 5,8-dibromoquinoxaline (0.5 mmol), and 5 ml of toluene were used to afford 205 mg of light green solid (88.6%). ^{1}H NMR ($CDCl_3$), δ (ppm): 0.81 (br, 6H), 0.95 (br, 4H), 1.19 (br, 12H), 2.10 (br, 4H), 7.71–8.04 (m, br, 8H), 8.93 (br, 2H). ^{13}C NMR ($CDCl_3$), δ (ppm): 14.07, 22.68, 24.20, 29.90, 31.58, 40.14, 55.22, 119.56, 125.65, 129.63, 130.23, 137.15, 140.38, 140.77, 141.43, 144.18, 151.21. Anal. Calcd for $C_{33}H_{36}N_2$ (%): C, 86.04; H, 7.88; N, 6.08. Found: C, 85.17; H, 7.81; N, 5.92.

2.2.3. Poly[2,7-(9,9′-dihexylfluorene)-alt-4,7-(2,1,3-benzothiadiazole)] (*PFBT*)

502 mg of 9,9-dihexylfluorene-2,7-bis(trimethyleneborate) (1 mmol), 294 mg of 4,7-dibromo-2,1,3-benzothiadiazole (1 mmol), and 10 ml of toluene were used to afford 420 mg of yellow solid (89.6%). ^{1}H NMR ($CDCl_3$), δ (ppm): 0.80 (br, 6H), 0.96 (br, 4H), 1.17 (br, 12H), 2.15 (br, 4H), 7.74–8.11 (m, br, 8H). ^{13}C NMR ($CDCl_3$), δ (ppm): 14.06, 22.61, 24.03, 29.80, 31.52, 40.25, 55.43, 120.05, 124.04, 127.98, 133.62, 136.47, 140.86, 151.77, 154.37. The peak positions of the NMR spectra are similar to that reported in the literature [12a]. Anal. Calcd for $C_{31}H_{34}N_2S$ (%): C, 79.79; H, 7.34; N, 6.00; S, 6.87. Found: C, 78.55; H, 7.39; N, 5.85; S, 6.58.

2.2.4. Poly[2,7-(9,9′-dihexylfluorene)-alt-5,7-(thieno[3,4-**b**]pyrazine)] (*PFTP*)

502 mg of 9,9-dihexylfluorene-2,7-bis(trimethyleneborate) (1 mmol), 294 mg of 5,7-dibromothieno[3,4-**b**]pyrazine (1 mmol), and 10 ml of toluene were used to afford 340 mg of deep purple solid (72.5%). ^{1}H NMR ($CDCl_3$), δ (ppm): 0.79 (br, 6H), 0.89 (br, 4H), 1.15 (br, 12H), 2.19 (br, 4H), 7.85–8.35 (m, br, 6H), 8.60 (m, br, 2H). ^{13}C NMR ($CDCl_3$), δ (ppm): 14.07, 22.57, 23.89, 29.72, 31.48, 40.51, 55.22, 120.39, 122.43, 127.30, 132.15, 132.80, 140.41, 140.62, 144.10, 151.97. Anal. Calcd for $C_{31}H_{34}N_2S$ (%): C, 79.78; H, 7.34; N, 6.00; S, 6.87. Found: C, 78.57; H, 7.52; N, 5.82; S, 6.37.

2.2.5. Poly[2,7-(9,9′-dihexylfluorene)-alt-5,7-(thieno[3,4-**b**]pyrazine)] (*PFTP0.5*)

502 mg of 9,9-dihexylfluorene-2,7-bis(trimethyleneborate) (1 mmol), 2.9 mg of 5,7-dibromothieno[3,4-**b**]pyrazine (0.01 mmol), 487.4 mg of 9,9-dihexyl-2,7-dibromofluorene (0.99 mmol), and 10 ml of toluene were used to afford 565 mg of red solid. ^{1}H NMR ($CDCl_3$), δ (ppm): 0.79 (br, 10H), 1.14 (br, 12H), 2.13 (br, 4H), 7.68–7.86 (m, br, 6H). ^{13}C NMR ($CDCl_3$), δ (ppm): 14.02, 22.56, 23.84, 29.67, 31.46, 40.35, 55.33, 119.97, 121.52, 126.15, 140.00, 140.53, 151.81. Anal. Calcd for $C_{24.905}H_{31.85}N_{0.01}S_{0.005}$ (%): C, 90.23; H, 9.68; N, 0.04; S, 0.05. Found: C, 89.07; H, 9.32; N, 0.03; S, 0.04.

2.2.6. Poly[2,7-(9,9′-dihexylfluorene)-alt-5,7-(thieno[3,4-**b**]pyrazine)] (*PFTP01*)

502 mg of 9,9-dihexylfluorene-2,7-bis(trimethyleneborate) (1 mmol), 5.9 mg of 5,7-dibromothieno[3,4-**b**]pyrazine (0.02 mmol), 482.5 mg of 9,9-dihexyl-2,7-dibromofluorene (0.98 mmol), and 10 ml of toluene were used to afford 570 mg of red solid. ^{1}H NMR ($CDCl_3$), δ (ppm): 0.80 (br, 10H), 1.15 (br, 12H), 2.13 (br, 4H), 7.68–7.86 (m, br, 6H). ^{13}C NMR ($CDCl_3$), δ (ppm): 14.02, 22.56, 23.85, 29.67, 31.46, 40.36, 55.33, 119.97, 121.52, 126.16, 140.02, 140.53, 151.81. Anal. Calcd for $C_{24.81}H_{31.7}N_{0.02}S_{0.01}$ (%): C, 90.15; H, 9.67; N, 0.08; S, 0.10. Found: C, 89.31; H, 10.03; N, 0.09; S, 0.11.

2.2.7. Poly[2,7-(9,9′-dihexylfluorene)-alt-5,7-(thieno[3,4-**b**]pyrazine)] (*PFTP05*)

502 mg of 9,9-dihexylfluorene-2,7-bis(trimethyleneborate) (1 mmol), 29.4 mg of 5,7-dibromothieno[3,4-**b**]pyrazine (0.1 mmol), 443 mg of 9,9-dihexyl-2,7-dibromofluorene (0.9 mmol), and 10 ml of toluene were used to afford 550 mg of purple–red solid. ^{1}H NMR ($CDCl_3$), δ (ppm): 0.80 (br, 10H), 1.14 (br, 12H), 2.13 (br, 4H), 7.68–8.32 (m, br, 6H), 8.63 (m, br, 0.096H). ^{13}C NMR ($CDCl_3$), δ (ppm): 14.02, 22.55, 23.84, 29.66, 31.45, 40.35, 55.32, 119.97, 121.58, 126.15,

140.00, 140.51, 141.35, 144.23, 151.80. Anal. Calcd for $C_{24.05}H_{30.5}N_{0.1}S_{0.05}$ (%): C, 89.54; H, 9.53; N, 0.43; S, 0.50. Found: C, 88.86; H, 9.09; N, 0.22; S, 0.44.

2.2.8. Poly[2,7-(9,9′-dihexylfluorene)-alt-5,7-(thieno[3,4-**b**] pyrazine)] (**PFTP15**)

502 mg of 9,9-dihexylfluorene-2,7-bis(trimethyleneborate) (1 mmol), 88 mg of 5,7-dibromothieno[3,4-**b**]pyrazine (0.3 mmol), 345 mg of 9,9-dihexyl-2,7-dibromofluorene (0.7 mmol), and 10 ml of toluene were used to afford 490 mg of purple-red solid. ^{1}H NMR ($CDCl_3$), δ (ppm): 0.79 (br, 10H), 1.14 (br, 12H), 2.13 (br, 4H), 7.80–8.33 (m, br, 6H), 8.61 (m, br, 0.328H). ^{13}C NMR ($CDCl_3$), δ (ppm): 14.02, 22.55, 23.85, 29.66, 31.45, 40.35, 55.44, 119.97, 121.52, 126.16, 140.01, 140.52, 141.62, 144.38, 151.81. Anal. Calcd for $C_{22.15}H_{27.5}N_{0.3}S_{0.15}$ (%): C, 87.87; H, 9.16; N, 1.39; S, 1.59. Found: C, 88.19; H, 8.95; N, 0.82; S, 1.30.

2.2.9. Poly[2,7-(9,9′-dihexylfluorene)-alt-5,7-(thieno[3,4-**b**] pyrazine)] (**PFTP25**)

502 mg of 9,9-dihexylfluorene-2,7-bis(trimethyleneborate) (1 mmol), 147 mg of 5,7-dibromothieno[3,4-**b**]pyrazine (0.5 mmol), 246 mg of 9,9-dihexyl-2,7-dibromofluorene (0.5 mmol), and 10 ml of toluene were used to afford 450 mg of deep purple solid. ^{1}H NMR ($CDCl_3$), δ (ppm): 0.80 (br, 10H), 1.16 (br, 12H), 2.14 (br, 4H), 7.70–8.34 (m, br, 6H), 8.61 (m, br, 0.627H). ^{13}C NMR ($CDCl_3$), δ (ppm): 14.02, 22.55, 23.84, 29.66, 31.46, 40.34, 55.38, 119.98, 121.52, 122.49, 126.17, 140.52, 141.21, 144.07, 151.84. Anal. Calcd for $C_{20.25}H_{24.5}N_{0.5}S_{0.25}$ (%): C, 85.97; H, 8.73; N, 2.47; S, 2.83. Found: C, 85.93; H, 8.77; N, 1.74; S, 2.75.

2.2.10. Poly[2,7-(9,9′-dihexylfluorene)-alt-5,7-(thieno[3,4-b] pyrazine)] (**PFTP35**)

502 mg of 9,9-dihexylfluorene-2,7-bis(trimethyleneborate) (1 mmol), 206 mg of 5,7-dibromothieno[3,4-*b*]pyrazine (0.7 mmol), 148 mg of 9,9-dihexyl-2,7-dibromofluorene (0.3 mmol), and 10 ml of toluene were used to afford 380 mg of deep purple solid. ^{1}H NMR ($CDCl_3$), δ (ppm): 0.82 (br, 10H), 1.25 (br, 12H), 2.36 (br, 4H), 7.83–8.35 (m, br, 6H), 8.60 (m, br, 1.111H). ^{13}C NMR ($CDCl_3$), δ (ppm): 14.00, 22.57, 23.73, 29.67, 31.48, 40.31, 55.45, 120.18, 121.44, 122.46, 132.45, 140.44, 142.34, 144.10, 151.82. Anal. Calcd for $C_{18.35}H_{21.5}N_{0.70}S_{0.35}$ (%): C, 83.77; H, 8.24; N, 3.73; S, 4.26.Found: C, 83.21; H, 8.05; N, 3.65; S, 4.36.

2.3. Characterization

^{1}H and ^{13}C nuclear magnetic resonance (NMR) data were obtained by a Bruker AV 500 MHz spectrometer. Gel permeation chromatographic analysis was performed on a Lab Alliance RI2000 instrument (two column, MIXED-C and D from Polymer Laboratories) connected with one refractive index detector from Schambeck SFD Gmbh. All GPC analyses were performed on polymer/THF solution at a flow rate of 1 ml/min at 40 °C and calibrated with polystyrene standards.

Thermogravimetric analysis (TGA) and differential scanning calorimetry (DSC) measurements were performed under a nitrogen atmosphere at a heating rate of 20 and 10 °C/min using a TA instrument TGA-951 and DSC-910S, respectively. UV–visible absorption and photoluminescence (PL) spectra were recorded on a Jasco model UV/VIS/NIR V-570 spectrometer and Fluorolog-3 spectrofluorometer (Jobin Yvon), respectively. For the solution spectra, polymers were dissolved in THF (ca. 10^{-6} M) and then put in a quartz cell for measurement. For the thin film spectra, polymers were first dissolved in THF (1 wt%) and then spin-coated on glass substrate at 1000 rpm for 30 s. Then, the thin film samples were dried at 60 °C under vacuum for measurement. Films used for the PL efficiency measurement were drop-coated from THF solution onto quartz substrates (ca. 1 wt%). PL efficiencies of polymer films on quartz substrates were measured using fluorolog 3 in combination with integrating sphere with 380 nm excitation.

The electrochemical properties of the polymer films were investigated on a Princeton Applied Research Model 273A Potentiostat/Galvanostat with a 0.1 M acetonitrile (99.5+%, Tedia) solution containing tetrabutylammonium tetrafluoroborate ($TBABF_4$) (Fluka, >99.9%) as the electrolyte. Platinum wire and rod-tip electrodes were used as counter and working electrodes respectively. Silver/silver ion (Ag in 0.1 M $AgNO_3$ (Acros, 99.8%) in the supporting electrolyte solutions) was used as a reference electrode. A 3 wt% solution of a polymer in THF or DMSO was used to prepare the polymer film on the Pt rod-tip electrode. Then, the cyclic voltammetry of films was performed on a three-electrode cell. The reference electrode was calibrated through by the cyclic voltammetry of ferrocene without any polymer added into the solution. The cyclic voltammograms were obtained at a voltage scan rate of 50 mV/s. The potential values obtained versus Fc^+/Fc standard were converted to the saturated calomel electrode (SCE) scale by adding a constant voltage to them. The energy parameters EA and IP were estimated from the measured redox potentials on the basis of the prior work on conjugated polymers which has shown that: IP=(E^{ox}_{onset}+4.4) and EA=(E^{red}_{onset}+4.4), where the onset potentials are in volts (vs. SCE) and IP and EA are in electron volts. The 4.4 eV constant in the relation among IP, EA, and redox potentials is the SCE energy level versus vacuum [13,31]. The electronic structure parameters, HOMO and LUMO, were estimated with the relation of HOMO=−IP and LUMO=−EA by assuming no configuration interactions.

2.4. Device fabrication and testing

The electroluminescent (EL) devices were fabricated on indium–tin oxide (ITO) coated glass substrate with sheet resistance of 20–30 Ω/sq. The substrate was ultrasonically cleaned with detergent, deionized water, acetone, and methanol, subsequently. Onto the ITO glass a layer of poly(ethylene dioxythiophene):poly(styrene sulfonate) (PEDOT:PSS), 50–60 nm thick (probed by Alpha-Step® 500 Surface Profiler), was formed by spin-coated from its aqueous

solution (Baytron P 8000, Bayer). The emissive layer was spin-coated at 1500 rpm from the corresponding p-xylene solution (1.5 wt%) on top of the vacuum-dried PEDOT:PSS layer. The nominal thickness of the emissive layer was 60–70 nm. Under a base pressure below 2×10^{-4} Torr, a layer of Ca (10 nm) was vacuum deposited as cathode and a thick layer of Ag (100 nm) was deposited subsequently as the protecting layer. The cathode area defines the active area of the device, which is 0.1256 cm^2 in this study.

Current–voltage characteristics were measured with a computerized Keithley 2400 source measure unit. The luminance and CIE coordinate of device were measured with Konica-Minolta Chroma Meter CS-100A. The EL spectrum of device was recorded on Fluorolog-3 spectrofluorometer (Jobin Yvon).

3. Results and discussions

3.1. Structural characterization of fluorene-based donor–acceptor copolymers

Fig. 1(a) and (b) shows the ^{1}H NMR spectra of **PFQ** and **PFTP** in $CDCl_3$, respectively. The signals in the ranges of

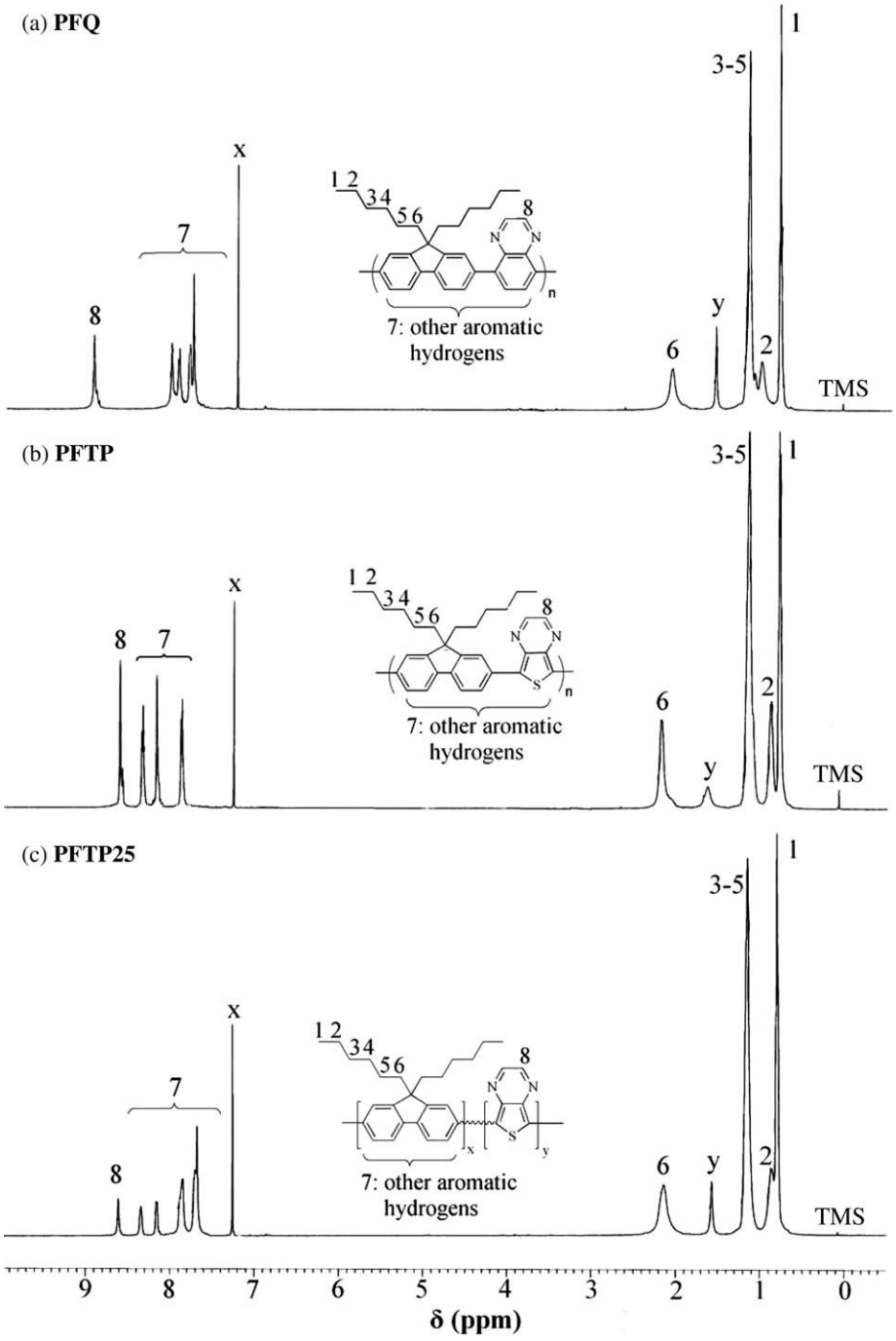

Fig. 1. ^{1}H NMR spectrum of the (a) **PFQ**; (b) **PFTP**; (c) **PFTP25** in $CDCl_3$, in which labels of x and y are $CHCl_3$ and H_2O, respectively.

Table 1
Molecular weights and thermal properties of the studied polymers

	M_n ($\times 10^3$)	PDI	T_g (°C)	T_d (°C)[a]	Acceptor ratio (%)	
					Theoretical	Exp.[b]
PF	57	3.41	67	409	0	0
PFQ	19	1.87	132	446	50	49.1
PFBT	19	2.10	115	434	50	48.5
PFTP	9	1.47	160	447	50	47.4
PFTP0.5	40	3.03	105	432	0.5	0.4
PFTP01	37	2.95	104	434	1	1.1
PFTP05	33	2.56	108	442	5	4.4
PFTP15	31	2.48	113	446	15	13.9
PFTP25	25	2.03	130	445	25	24.4
PFTP35	11	1.52	137	446	35	35.6

[a] 95 wt% residue temperature.
[b] Estimated from results of elemental analysis.

0.79–2.19 and 7.71–8.04 ppm are assigned to the hexyl and phenylene protons, respectively. The signals assigned to protons on the **Q** and **TP** segments are around 8.93 and 8.60 ppm, respectively. The numbers of protons estimated from the integration of peaks are in good agreement with the proposed structures. The ^{13}C NMR results also support the proposed chemical structures of **PFQ** and **PFTP**. Fig. 1(c) shows the ^{1}H NMR spectrum of **PFTP25** in $CDCl_3$. The signals assigned to the phenylene protons at 7.70–8.34 ppm split into four peaks instead of three peaks in Fig. 1(b), which could be attributed to the random arrangement of fluorene and **TP** segments on the backbone. The actual content of the **TP** segments on the backbone was estimated based on the N and S contents obtained in the elemental analysis, which are listed in Table 1. As shown in the table, the theoretical and experimental acceptor contents are in a good agreement.

The resulted copolymers (**PFQ**, **PFBT**, **PFTP**, and **PFTP0.5–PFTP35**) are readily soluble in $CHCl_3$, THF, and toluene. The molecular weights of these copolymers are listed in Table 1. The number-averaged molecular weights and polydispersity indices (M_n, PDI) of the **PFQ**, **PFBT**, and **PFTP** are (18970, 1.87), (19229, 2.10), and (8900, 1.47), respectively. The M_n of the **PFTP0.5–PFTP35** decreases with increasing the **TP** content, which could be attributed to poor solubility or reactivity of the **TP** monomers in toluene. The experimental carbon, hydrogen, and nitrogen content of the synthesized polymers are in a good agreement with the theoretical values, which indicates the successful preparation of the proposed polymers.

3.2. Thermal properties

Fig. 2 shows the TGA (insert figure) and DSC curves of the **PF**, **PFQ**, **PFBT**, and **PFTP**, respectively. The thermal decomposition temperatures (T_d, 95 wt% residue) and glass transition temperatures (T_g) estimated from their TGA and DSC curves are summarized in Table 1, respectively. The T_d of the **PFQ**, **PFBT**, and **PFTP** are 446, 434, and 447 °C, respectively, which are higher than that of the parent **PF** with 409 °C. As shown in Fig. 2, the T_g of the **PF**, **PFQ**, **PFBT**, and **PFTP** are 67, 132, 115, and 160 °C, respectively. The T_g of

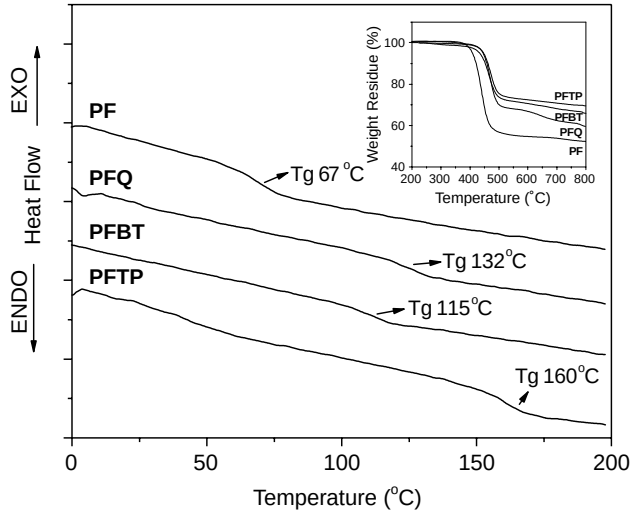

Fig. 2. DSC curves of the **PF**, **PFQ**, **PFBT**, and **PFTP** at a heating rate of 10 °C/min under a nitrogen atmosphere. The insert shows the TGA curves of the above polymers at a heating rate of 20 °C/min under a nitrogen atmosphere.

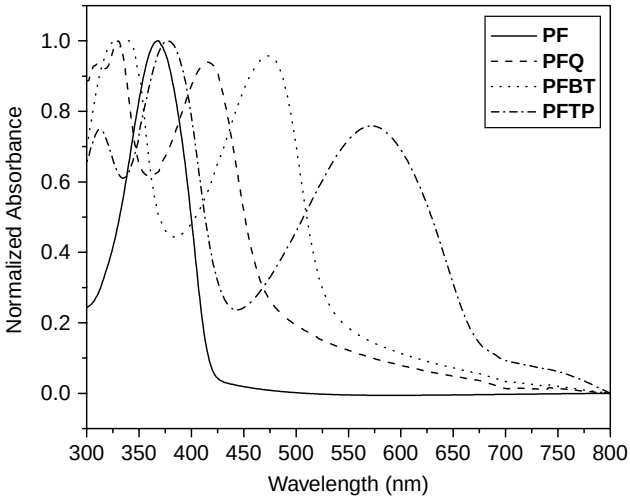

Fig. 3. Normalized UV–vis absorption spectra of the **PF**, **PFQ**, **PFBT**, and **PFTP** films.

Table 2
Optical properties of the studied polymers

	λ_{max}^{abs} (film) (nm)	E_g^{opt} (eV)[a]	λ_{max}^{PL} (soln[b]) (nm)	λ_{max}^{PL} (film) (nm)	Ψ^{PL} (%)
PF	368	2.95	412, 437	424, 445,	56.6
PFQ	416	2.64	488	493	22.4
PFBT	470	2.34	532	540	18.5
PFTP	378, 578	1.82	646	439, 508, 674	2.1
PFTP0.5	381	2.95	415, 440	425, 446, 620	37.3
PFTP01	382	2.02	415, 440	425, 446, 629, 655	25.3
PFTP05	381, 530	1.98	414, 440, 634	449, 474, 635, 655	11.3
PFTP15	382, 540	1.94	414, 439, 636	450, 640, 654	6.9
PFTP25	381, 551	1.90	416, 439, 640	659	5.1
PFTP35	382, 578	1.82	416, 440, 642	439, 510, 669	3.7

[a] Estimated from the absorption edge of the thin film.
[b] In THF dilute solution (ca. 10^{-6} M).

the fluorene-**TP** copolymers increases with increasing the **TP** content from the 105 °C of **PFTP0.5** to 137 °C of **PFTP35**. It suggests that the thermal properties of the **PF** can be elevated by incorporating the acceptor moiety on the backbone, which might be important for device applications.

3.3. Optical absorption and electrochemical characteristics

The UV–visible absorption spectra of the **PF**, **PFQ**, **PFBT**, and **PFTP** films are shown in Fig. 3, and the corresponding absorption maximum (λ_{max}) are summarized in Table 2. The λ_{max} of the **PF**, **PFQ**, **PFBT**, and **PFTP** films are 368, 416, 470, and 578 nm, respectively. It suggests that the optical properties of these polymers could be tuned over a wide range through different acceptors. The optical band gaps (eV) estimated from the absorption edges are in the order of **PF** (2.95) > **PFQ** (2.64) > **PFBT** (2.34) > **PFTP** (1.82). Note that the optical band gap of the **PFBT** is in a good agreement with that of 2.40 eV reported in literature [32]. The much lower band gaps of the **PFQ**, **PFBT**, and **PFTP** than that of the parent **PF** are probably due to the intramolecular charge transfer between the fluorene and acceptor or the backbone planarity. However, the decrement of band gaps of these alternating copolymers is not in consistence with the increasing order of the acceptor strength. As described in the introduction section, the electron-accepting strength is in the order of **BT** > **TP** > **Q** [25]. The smaller band gap of the **PFTP** than that of the **PFBT** might be because of the backbone planarity. The **TP** with the five member thiophene ring results in a smaller torsional angle with fluorene than that of the **BT** with the six-member phenylene ring, which assists the efficient intramolecular charge transfer and results in a smaller band gap. The extended tails and/or shoulders near the absorption edges of **PFQ**, **PFBT**, and **PFTP** suggest stronger inter-chain interaction as compared to the parent **PF**. This could also result in a smaller band gap.

The UV–visible absorption spectra of the **PF**, **PFTP**, and **PFTP0.5**–**PFTP35** films are shown in Fig. 4, and the corresponding λ_{max} are summarized in Table 2. Two absorption peaks are observed in the absorption spectra of the copolymers. The short-wavelength absorption peaks around 380 nm could be attributed to the **PF** segment as compared to that of the **PF**. The λ_{max} (519–578 nm) and intensities of the long-wavelength absorption peaks increase with increasing the **TP** content, implying that this band is probably attributed to the **TP** segment. As the TP content increases, the extender tails and/or shoulders near the absorption edges become more obvious, suggesting the extent of inter-chain interaction increasing with acceptor content on the backbone.

The oxidation and reduction potentials of these polymers were investigated by cyclic voltammetry. Fig. 5 represents the cyclic voltammograms of the **PF**, **PFQ**, **PFBT**, and **PFTP**. The **PFBT** exhibits quasi reversible oxidation and reduction. However, the electrochemical oxidation of the **PFQ** and **PFTP** is not reversible under the experimental conditions. The electrochemical oxidation and reduction potentials and the electronic structure parameters are summarized in Table 3. The HOMO and LUMO levels of the **PF** are −5.39 and −2.44 eV, respectively. The HOMO levels of the **PFQ**, **PFBT**, and **PFTP** are in the range of −5.13 to −5.51 eV, which are similar to that of the **PF**. However, the LUMO levels of these alternating copolymers are smaller than that of the **PF**,

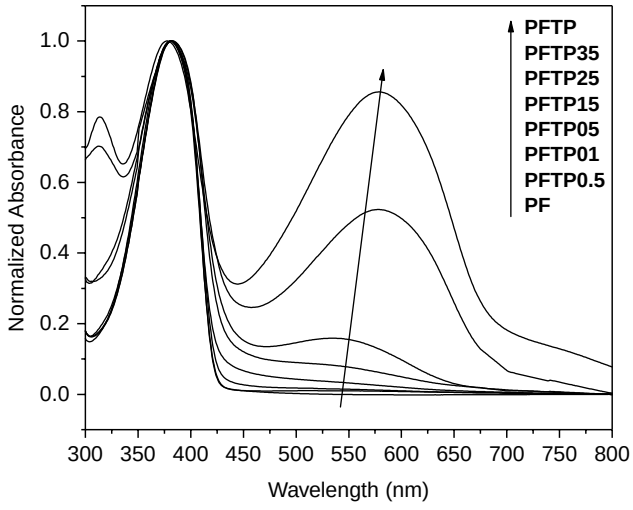

Fig. 4. Normalized UV–vis absorption spectra of the **PF**, **PFTP**, and **PFTP0.5**–**PFTP35** films on glass substrates.

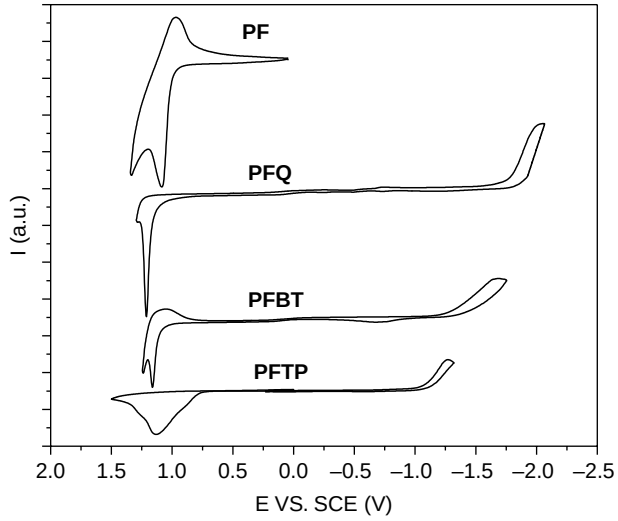

Fig. 5. Cyclic voltammograms of the **PF**, **PFQ**, **PFBT**, and **PFTP** films on platinum in M acetonitrile (99.5+%, Tedia) solution containing tetrabutylammonium tetrafluoroborate ($TBABF_4$) (Fluka, >99.9%) as the electrolyte.

which are −2.65, −3.14, and −3.33 eV for the **PFQ**, **PFBT**, and **PFTP**, respectively. It suggests that the incorporation of the acceptor moiety increases the electron affinity. The electrochemical band gaps estimated from the difference of the obtained HOMO and LUMO levels are 2.86, 2.35, and 1.80 eV for **PFQ**, **PFBT**, and **PFTP**, respectively, which has the trend as the optical band gap variation. It also demonstrates the more efficient intramolecular charge transfer of the **PFTP** than that of the other two polymers. The electrochemical characteristics of **PFTP0.5–PFTP35** are summarized in Table 3. The onset oxidation and reduction potentials of the **PFTP0.5–PFTP35** vary between 0.73 (**PFTP**)–0.99 and −1.07 (**PFTP**) to −1.34 V, respectively. The HOMO level of the **PFTP0.5–PFTP35** does not show a significant variation except that of the **PFTP35** with −5.25 eV. The LUMO levels decrease from −3.07 eV to −3.33 eV as the **TP** content increasing from 0.5 to 50%, which also indicates the incorporation of the acceptor moiety on the polymer backbone.

3.4. Photoluminescence properties

Fig. 6 shows the photoluminescence spectra of the **PF**, **PFQ**, **PFBT**, and **PFTP** in solid-state films excited at the wavelength of 380 nm, of which the corresponding emission maxima (λ_{max}^{PL}) are summarized in Table 2. The λ_{max}^{PL} of the **PF**, **PFQ**, **PFBT**, and **PFTP** in THF are 412, 488, 532, and 646 nm, respectively, while those in solid-state films are 445, 493, 540, and 674 nm. The λ_{max}^{PL} of the **PFBT** at 2.33 eV (532 nm) in THF is in good agreement with that at 2.30 eV reported in literature [32]. The variation of emission peaks shows the same trend as that of optical absorption spectra. The emissive colors of the **PF**, **PFQ**, **PFBT**, and **PFTP** are blue, green, yellow, and red, respectively, which cover the entire visible region. The above results suggest that the color tuning of the fluorene-based alternating copolymers by incorporating different acceptor segments in the backbone is feasible. Two additional emission peaks of the **PFTP** at 439 and 508 nm are observed in the solid state but not shown in dilute solution. They are probably attributed to the intermolecular interaction of the fluorene segments and the formation of excimers in the solid state, respectively, as compared to the PL spectrum of the **PF**

The photoluminescence characteristics of the **PFTP** in dilute solution (ca. 10^{-6} M) were investigated in different solutions with increasing solvent polarity of triethylamine (TEA), toluene, THF, $CHCl_3$, and $CHCl_3/CH_3OH$ (volume ratio = 1:1). The corresponding λ_{max}^{PL} on the above solvents are at 627, 633, 646, 667, and 678 nm, respectively. It suggests that the λ_{max}^{PL} could increase up to 51 nm with increasing the solvent polarity. Such positive solvatochromism indicates a significant intramolecular charge transfer excited in the **PFTP** [33,34]. Similar phenomena of positive solvatochromism on photoluminescence were also observed in the **PFQ** and **PFBT** but with smaller red shifts of 33 and 31 nm, respectively. Hence, it indicates that more efficient intramolecular charge transfer in the **PFTP** than the other two polymers from the above result.

Fig. 7(a) and (b) shows the photoluminescence spectra of the **PF**, **PFTP**, and **PFTP0.5–PFTP35** excited at the wavelength of 380 nm in THF and solid state film,

Table 3
Electrochemical properties of the studied polymers

	Oxidation (vs. SCE)			Reduction (vs. SCE)			E_g^{ec} (eV)[a]
	E_{pa} (V)	E_{onset} (V)	HOMO (eV)	E_{pc} (V)	E_{onset} (V)	LUMO (eV)	
PF	1.13	0.99	−5.39	–	–	−2.44[b]	–
PFQ	1.21	1.11	−5.51	−2.06	−1.75	−2.65	2.86
PFBT	1.16	1.09	−5.49	−1.68	−1.26	−3.14	2.35
PFTP	1.18	0.73	−5.13	−1.30	−1.07	−3.33	1.80
PFTP0.5	1.55	0.98	−5.38	−1.78	−1.33	−3.07	2.31
PFTP01	1.20	0.97	−5.37	−1.80	−1.34	−3.06	2.31
PFTP05	1.22	0.97	−5.37	−1.82	−1.33	−3.07	2.30
PFTP15	1.21	0.99	−5.39	−1.49	−1.20	−3.20	2.19
PFTP25	1.32	0.95	−5.35	−1.55	−1.18	−3.22	2.13
PFTP35	1.05	0.85	−5.25	−1.45	−1.16	−3.24	2.01

[a] The electrochemical band gap, E_g^{ec} = LUMO − HOMO.
[b] Estimated by the relation of LUMO = E_g^{opt} + HOMO.

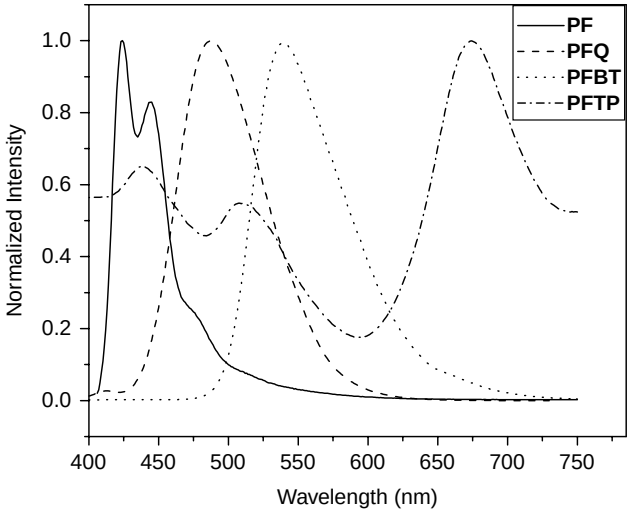

Fig. 6. Normalized PL spectra of the **PF**, **PFQ**, **PFBT**, and **PFTP** in solid state films.

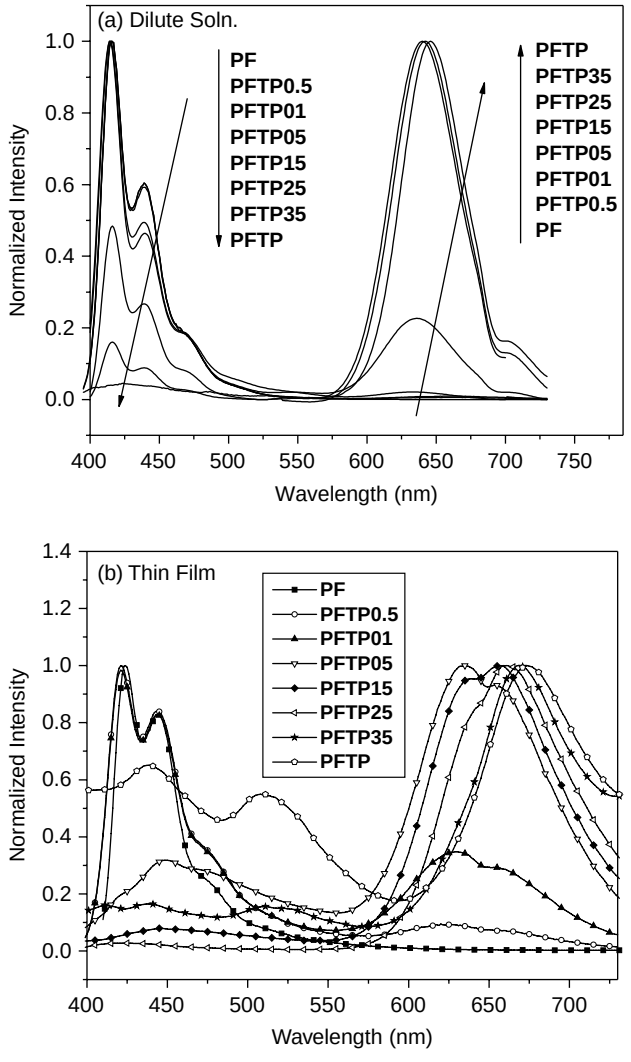

Fig. 7. (a) Normalized PL spectra of the **PFTP0.5–PFTP35** in THF (ca. 10^{-6} M) and (b) solid state films, respectively.

respectively, of which the corresponding λ_{max}^{PL} are summarized in Table 2. As shown in Fig. 7(a), the PL spectra of the **PFTP0.5** and **PFTP01** in dilute solution are dominated by emission from the **PF** segments. As the **TP** content increases to the **PFTP05**, a tiny additional emission peak is observed at 634 nm as compared to that of **PF**. The intensity of such emission peak increases with increasing the **TP** content from 5–50% and undergoes a red shift from 634–646 nm. It indicates that this long-wavelength emission peak is attributed to the **TP** segment. The increasing intensity of the long-wavelength peak with increasing **TP** content also suggests that energy transfer from the excited state of the **PF** to the **TP** segments [19]. This energy transfer was also observed in similar systems of fluorene with different comonomers, including 2,1,3-benzoselenadiazole, 4,7-di-2′-thienyl-2,1,3-benzothiadiazole, 2,1,3-naphtho-selenadizole, 4,7-di(2′-selenophenyl)-2,1,3-benzothiadiazole, and 4,7-di(2′-selenophenyl)-2,1,3-benzoselenadiazole, in the literatures [19,35–37]. The PL spectra of the **PF**, **PFTP**, and **PFTP0.5–PFTP35** films shown in Fig. 7(b) also exhibit two emission peaks around 430 and 640 nm, corresponding to the **PF** and **TP** segments, respectively. As compared to Fig. 7(a), the long-wavelength emission peaks of these polymer films undergo a red shift for 1–28 nm from those in THF. The long-wavelength peak at 620 nm is observed at the relatively low **TP** content of 0.5% in solid state, in comparison with the absence of this peak of **FTP0.5** in dilute solution. It indicates that interchain energy transfer plays an important role in solid state. The relative intensities of the long-wavelength to short-wavelength emission peak in Fig. 7(b) increases first from **PFTP0.5** to **PFTP25** and then decreases with increasing **TP** content. The PL characteristics of these copolymers in solid state could be influenced by two competing effects: Förster energy transfer and the intramolecular charge transfer/heavy-atom fluorescence quenching. As increasing the **TP** content, it increases the energy transfer from the **PF** to **TP** segments and results in an enhancement of the long-wavelength peak. However, the fluorescence quenching due to the intramolecular charge transfer/heavy-atom effect arisen from **TP** segments also becomes more pronounced as the **TP** content larger than 35%.

The energy transfer between the **PF** and **TP** segments was further studied by the PL spectra of the **PFTP15** in THF with different concentrations of 5×10^{-7}–1×10^{-4} M, as shown in Fig. 8. Even in a very dilute concentration of 5×10^{-7} M (low enough to avoid a strong interchain energy transfer), the long-wavelength emission peak contributed by the **TP** segment could be observed. It indicates relatively efficient intrachain energy transfer between **PF** and **TP** segment. The relative intensities of the long-wavelength to short-wavelength emission peak increase with increasing solution concentration. The short-wavelength emission peak contributed by the **PF** segments is completely quenched when the concentration is equal to or greater than 5×10^{-5} M. This suggests that the energy transfer between **PF** and **TP** segments also happens via interchain mechanism.

Table 2 also lists the PL efficiencies of the studied polymer films. The PL efficiencies of the **PF**, **PFQ**, **PFBT**, and **PFTP**

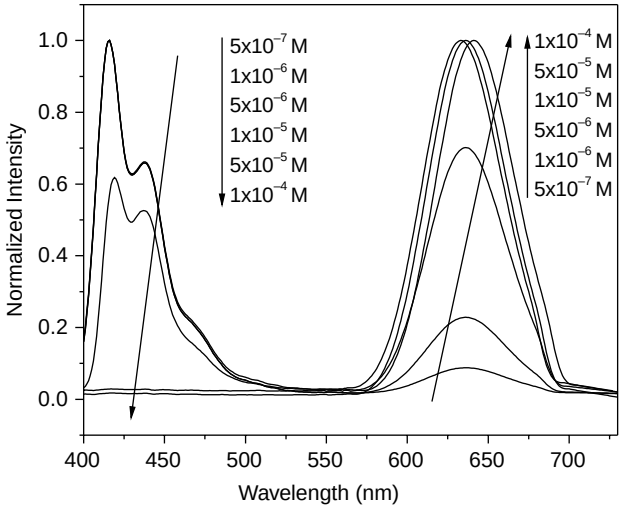

Fig. 8. Normalized PL spectra of the **PFTP15** in THF solution with different concentrations of 5×10^{-7}–1×10^{-4} M.

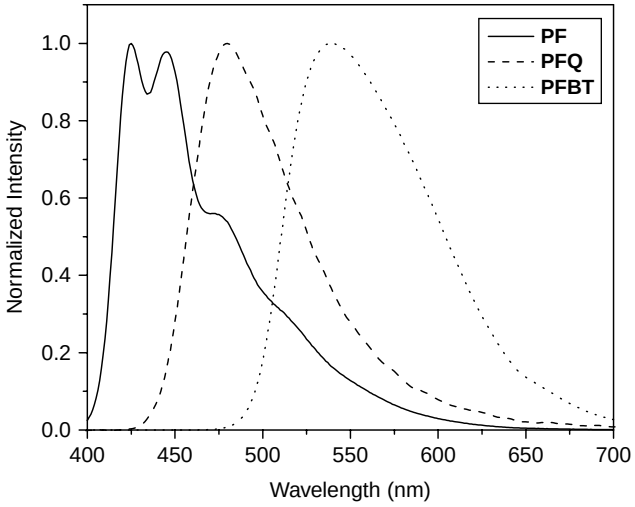

Fig. 9. EL spectra using the **PF**, **PFQ**, and **PFBT** as the emissive layer.

are 56.6, 22.4, 18.5, and 2,1%, respectively. The PL efficiency shows a dramatic decrease after the incorporation of acceptor segments on the backbone. It suggests that the PL efficiencies decrease by increasing intramolecular charge transfer, which is similar to those reported in the literature [33,38]. Another possibility of the poor PL efficiencies on the **PFTP** could also be attributed to the heavy-atom effect of the sulfur on the thiophene ring, which increases the intersystem crossing of singlet and triplet which results in the loss of PL efficiency [16]. The PL efficiencies of the random copolymers**, PFTP0.5**–**PFTP35** also decrease with increasing the **TP** content on the main chain but higher than the alternating copolymer, **PFTP** due to the reducing intramolecular charge transfer or heavy-atom effect. Similar variation on the PL efficiencies was also observed for the copolymers derived from 9,9-dioxylfluorene and 4,7-di-2′-thienyl-2,1,3-benzothiadiazole [35]. The higher PL efficiencies of random copolymers than those of alternating copolymers suggest that the incorporation of very small amount of acceptor is more favorable in consideration of efficient light-emitting device applications.

3.5. Electroluminescence (el) characteristics

EL devices with the studied polymers as emissive layers were fabricated with configuration ITO/PEDOT:PSS/emissive layer/Ca/Ag. Fig. 9 shows the EL spectra of the EL devices with the **PF**, **PFQ**, and **PFBT** as the emissive layer, respectively. The emission maxima (λ_{max}^{EL}) of EL devices based on the **PF**, **PFQ**, and **PFBT** are 425, 480, and 540 nm, respectively, which are similar to the corresponding λ_{max}^{PL} shown in Fig. 6. This result suggests that the color tuning on the EL devices of polyfluorenes through incorporation various acceptors on the backbone is feasible. However, the EL device with the **PFTP** as the emissive layer was too weak to be detected. It is probably due to the intramolecular charge transfer or heavy-atom effect resulting in fluorescence quenching as described previously. Fig. 10 shows the EL spectra using the random copolymers of **PFTP0.5**–**PFTP25** as the emissive layer. The EL device with the **PFTP35** as emissive layer is too weak to be detected, which is attributed to the same reason in the case of the **PFTP**. As shown in the figure, the emission maxima are red-shifted from 632 nm of the **PFTP0.5** to 667 nm of the **PFTP25**. Besides, only red emission is observed in the EL spectra as the **TP** content greater than 1%, which is quite different from the corresponding PL spectra. Even for the EL device based on the **PFTP0.5**, the red emission from the **TP** segment is stronger than the blue emission from **PF** segment. The differences between the PL and EL spectra could be attributed to the differences in the recombination zone for photo- and electric excitations [39]. For the case of the PL, red emission arises from the Förster energy transfer from **PF** segment to **TP** segment. However, the dominant red emission in EL arises from the charge trapping mechanism. The **TP** segment serves as an efficient electron trap, and the generated excitons are efficiently confined on **TP** segment. Therefore, blue emission are completely quenched even the **TP** content as

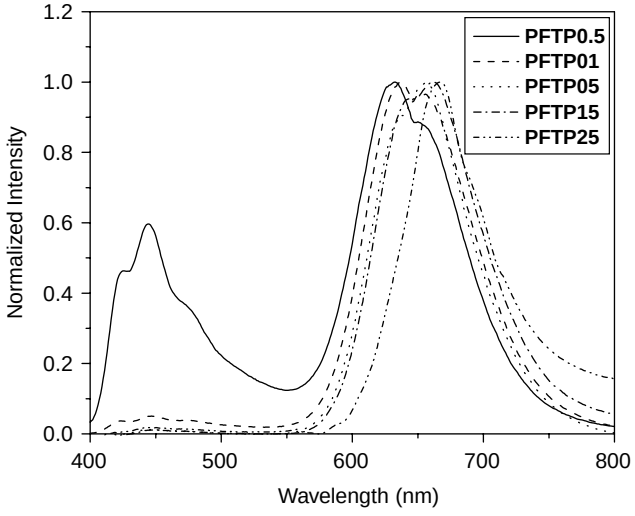

Fig. 10. EL spectra using the **PFTP0.5**–**PFTP25** as the emissive layer.

Table 4
Luminescence characteristics of the studied polymers

	λ_{max}^{EL} (nm)	Bias (V)	Current density[a] (mA/cm^2)	Luminance (cd/m^2)	Luminance yield (cd/A)	EQE$_{max}$ (%)	Chromaticity coordinate[b]	
							x	*y*
PF	425, 445, 475	10.5	54.7	103	0.188	0.18	0.221	0.264
PFQ	480	8.5	24.5	93.3	0.381	0.20	0.228	0.397
PFBT	540	7	58.1	623	1.07	0.13	0.430	0.559
PFTP	N/A	N/A	N/A	N/A	N/A	N/A	N/A	N/A
PFTP0.5	425, 445, 632	12	39.9	61.1	0.153	0.14	0.545	0.302
PFTP01	638	12.5	43.8	175	0.399	0.48	0.660	0.312
PFTP05	656	14	28.6	18.9	0.066	0.08	0.659	0.317
PFTP15	662	12	29.4	10.2	0.035	0.04	0.664	0.320
PFTP25	667	10.5	24.3	6.3	0.026	0.03	0.701	0.299
PFTP35	N/A	N/A	N/A	N/A	N/A	N/A	N/A	N/A

Device structure: ITO/PEDOT:PSS/emissive layer/Ca/Ag. Measured at maximum luminance yield.
[a] Active area is 0.1256 cm^2.
[b] The commission Internationale de L'Eclairage (CIE) 1931 coordinates.

low as 1%. It has been shown for the intramolecular trapping systems [19] that the hole and electron trapping mechanism is most favorable if the HOMO level of the guest is above that of the host and if LUMO level of the guest is below that of host [40]. As discussed in the electrochemical characteristics, the HOMO levels of the **PFTP0.5–PFTP25** is almost the same as that of the **PF** but the LUMO levels are lower. Therefore, electron trapping is highly favorable in the EL devices based on the **PFTP0.5–PFTP25**.

Table 4 lists the EL characteristics using the studied polymers as emissive layer. The external quantum efficiency (EQE) of the **PF**, **PFQ**, and **PFBT** are 0.18, 0.20, and 0.13%, respectively, which shows a different trend with the corresponding PL efficiencies of 56.6, 22.4, and 18.5%. It has been discussed previously that the PL efficiency may decrease with increasing intramolecular charge transfer between fluorene and acceptor segments. However, the EQE of the **PFQ** is greater than that of the **PF**. It is probably attributed to the LUMO levels of the **PFQ** (−2.65 eV) and **PF** (−2.44 eV) compared with the work function of the calcium cathode (2.87 eV). The lower the LUMO level, the smaller electron-injection barrier lays between the emissive layer and calcium cathode, which results in a higher EQE of **PFQ**. For the EL characteristics based on the **PFTP0.5–PFTP25**, there are two competing factors for the variation of EQE: the LUMO level and intramolecular charge transfer or heavy-atom effect. The EQE increases first from 0.14–0.48% as the **TP** content increases from 0.5–1% but then decrease rapidly at a higher **TP** content. As mentioned in the previous section, both fluorescence quenching due to intramolecular charge transfer or heavy-atom effect lower the PL efficiencies of these copolymers with increasing **TP** content. However, the **TP** segment could lower the LUMO level and facilitate electron transporting. The LUMO level decreases from −3.07 to −3.33 eV as **TP** content increasing from 0.5–35%, which results in decreasing electron-injection barrier with increasing **TP** content. These two competing effects result in an optimum EQE using **FTP01** as emissive layer. Nevertheless, the better EQE of the fluorene-**TP** random copolymers than that of the **FTP** alternating copolymer suggest that color tuning and enhanced device performance could be accomplished with incorporating a very small amount of acceptor on the backbone. The commission Internationale de L'Eclairage (CIE) 1931 coordinates of the LEDs with **PFQ**, **PFBT**, and **PFTP01** as emissive layers under the condition of maximum EQE are (0.228, 0.397), (0.430, 0.559), and (0.660, 0.312), respectively. The standard red and green demanded by the National Television System Committee (NTSC) are (0.66, 0.34) and (0.26, 0.65), respectively. The emissive color of **PFTP01** is almost identical to the standard red demanded by the NTSC. However, the emissive color of **PFQ** is blue-green rather than the standard green demanded by the NTSC. Further modification of acceptor strength will be required to fulfill the standard green emission. Nevertheless, the emission maxima as well as the CIE coordinates listed in Table 4 suggest the successful color tuning of fluorene-based donor–acceptor copolymers by incorporation of different acceptor segments.

4. Conclusions

Three fluorene-acceptor alternating copolymers (**PFQ**, **PFBT**, **PFTP**) and six fluorene-**TP** (**PFTP0.5–PFTP35**) random copolymers were prepared and characterized. The experimental results suggest that the acceptor strength or content significantly affect the electronic and optoelectronic properties due to the acceptor strength or intramolecular charge transfer, including the optical band gap, LUMO level, and luminescence maximum. The emission maxima of the photoluminescence spectra on the **PF**, **PFQ**, **PFBT**, and **PFTP** films corresponding to the color of blue, green, yellow, and red, respectively. The significant positive solvatochromism on the PL spectra in different polar solvents suggests that the efficient intramolecular charge transfer in **PFTP**. However, such charge transfer or heavy-atom effect results in fluorescence quenching and thus reduces the PL efficiencies. By random copolymerizing the **TP** into the **PF**, the PL efficiency

could be improved. A significantly reduction on the **PF** emission peak with increasing the **TP** content of the **PFTP0.5**–**PFTP35** suggests the energy transfer between the **PF** and **TP** segments. Besides, the characteristics of the electroluminescence devices suggest that such energy transfer results in the complete quenching of the **PF** emission as only 1% **TP** content (**PFTP01**). The maximum external quantum efficiency (EQE) of the EL device based on the **PFTP01** is superior to that of the **PF** due to a better matching of the LUMO level with the calcium cathode. The CIE 1931 coordinates of the **PFTP01** based EL devices under the condition of maximum EQE is (0.66, 0.31), which is close to the standard red of (0.66, 0.34). The luminescence characteristics based on the prepared polymers depend on the Förster energy transfer or the intramolecular charge transfer, or heavy-atom fluorescence quenching. The present study suggests that the tuning of the electronic and optoelectronic properties could be achieved by incorporating various acceptors or content into the polyfluorenes.

Acknowledgements

This work was supported by the National Science Council and the Ministry of Economic Affairs of Taiwan, ROC. We thank Mr Yi-Chih Tung for the technical assistance for preparing the **PFQ** sample.

References

[1] Burroughes JH, Bradley DDC, Brown AR, Marks RN, Mackay K, Friend RH, et al. Nature 1990;347:539.
[2] Kraft A, Grimsdale AC, Holmes AB. Angew Chem, Int Ed 1998;37:402.
[3] Halls JJM, Walsh CA, Greenham NC, Marseglia EA, Friend RH, Moratti SC, et al. Nature 1995;376:498.
[4] Yu G, Gao J, Hummelen JC, Wudl F, Heeger AJ. Science 1995;270:1789.
[5] Yang Y, Heeger AJ. Nature 1994;372:344.
[6] Sirringhaus H, Tessler N, Friend RH. Science 1998;280:1741.
[7] Babel A, Jenekhe SA. J Am Chem Soc 2003;125:13656.
[8] van Mullekom HAM, Vekemans JAJM, Havinga EE, Meijer EW. Mater Sci Eng 2001;32:1.
[9] Bredas JL, Heeger AJ, Wudl F. J Chem Phys 1986;85:4673.
[10] Banister AJ, Gorrel IB. Adv Mater 1998;10:1415.
[11] Yamamoto T, Zhou Z-H, Kanbara T, Shimura M, Kizu K, Maruyama T, et al. J Am Chem Soc 1996;118:10389.
[12] Akoudad S, Roncali J. Chem Commun 1998;2081.
[13] Zhang X, Jenekhe SA. Macromolecules 2000;33:2069.
[14] Liu CC, Tsai FC, Chang CC, Hsieh KH, Lin JJ, Chen WC. Polymer 2005; 46:4950.
[15] Lin WJ, Chen WC, Wu WC, Niu YH, Jen AKY. Macromolecules 2004; 37:2335.
[16] Herguth P, Jiang X, Liu MS, Jen AKY. Macromolecules 2002;35:6094.
[17] Liu SP, Chan HSO, Ng SC. J Polym Sci, A: Polym Chem 2004;42:4792.
[18] Kinder L, Kanicki J, Petroff P. Synth Met 2004;146:181.
[19] Yang J, Jiang C, Zhang Y, Yang R, Yang W, Hou Q, et al. Macromolecules 2004;37:1211.
[20] Sonar P, Zhang J, Grimsdale AC, Müllen K, Surin M, Lazzaroni R, et al. Macromolecules 2004;37:709.
[21] Kulkarni AP, Zhu Y, Jenekhe SA. Macromolecules 2005;38:1553.
[22] Ego C, Marsitzky D, Becker S, Zhang J, Grimsdale AC, Müllen K, et al. J Am Chem Soc 2004;125:437.
[23] Snaith HJ, Greenham NG, Friend RH. Adv Mater 2004;16:1640.
[24] Chua L-L, Zaumseil J, Chang J-F, Ou EC-W, Ho PK-H, Sirringhaus H, et al. Nature 2005;434:194.
[25] Kitamura C, Tanaka S, Yamashita Y. Chem Mater 1996;8:570.
[26] Pilgram K, Zupon M, Skiles RJ. Heterocycl Chem 1970;7:629.
[27] Naef R, Balli H. Helv Chim Acta 1978;61:2958.
[28] Yamamoto T, Sugiyama K, Kushida T, Inoue T, Kanbara T. J Am Chem Soc 1996;118:3930.
[29] Kenning DD, Mitchell KA, Calhoun TR, Funfar MR, Sattler DJ, Rasmussen SC. J Org Chem 2002;67:9073.
[30] Berlin A, Zanelli A. Chem Mater 2004;16:3667.
[31] Tsai FC, Chang CC, Liu CL, Chen WC, Jenekhe SA. Macromolecules 2005;38:1958.
[32] Campbell AJ, Bradley DDC, Antoniadis H. Appl Phys Lett 2001;79:2133.
[33] Jenekhe SA, Lu L, Alam MM. Macromolecules 2001;34:7315.
[34] Reichardt C. Chem Rev 1994;94:2319.
[35] Hou Q, Xu Y, Yang W, Yuan M, Peng J, Cao Y. J Mater Chem 2002;12: 2887.
[36] Yang R, Tian R, Hou Q, Yang W, Cao Y. Macromolecules 2003;36: 7453.
[37] Yang R, Tian R, Yan J, Zhang Y, Yang J, Hou Q, et al. Macromolecules 2005;38:244.
[38] Zhang QT, Tour JM. J Am Chem Soc 1998;120:5355.
[39] McGehee MD, Bergstedt TT, Zhang C, Saab AP, O'Regan MB, Bazan GC, et al. Adv Mater 1999;11:1349.
[40] Gong X, Ostrowski JC, Moses D, Bazan GC, Heeger AJ. Adv Funct Mater 2003;13:439.